ARTICLE

doi:10.1038/nature11360

A Cenozoic record of the equatorial Pacific carbonate compensation depth

A list of authors and their affiliations appears at the end of the paper.

Atmospheric carbon dioxide concentrations and climate are regulated on geological timescales by the balance between carbon input from volcanic and metamorphic outgassing and its removal by weathering feedbacks; these feedbacks involve the erosion of silicate rocks and organic-carbon-bearing rocks. The integrated effect of these processes is reflected in the calcium carbonate compensation depth, which is the oceanic depth at which calcium carbonate is dissolved. Here we present a carbonate accumulation record that covers the past 53 million years from a depth transect in the equatorial Pacific Ocean. The carbonate compensation depth tracks long-term ocean cooling, deepening from 3.0–3.5 kilometres during the early Cenozoic (approximately 55 million years ago) to 4.6 kilometres at present, consistent with an overall Cenozoic increase in weathering. We find large superimposed fluctuations in carbonate compensation depth during the middle and late Eocene. Using Earth system models, we identify changes in weathering and the mode of organic-carbon delivery as two key processes to explain these large-scale Eocene fluctuations of the carbonate compensation depth.

The Pacific, as the world's largest ocean, is intricately involved in the prominent changes in the global carbon cycle and climate system that took place during the Cenozoic[1]. The equatorial Pacific makes a disproportionally large global contribution to biogenic sediment burial in the pelagic realm due to equatorial upwelling, and thus plays an important part in climate regulation[1]. Expeditions 320 and 321 of the Integrated Ocean Drilling Program (IODP), the 'Pacific Equatorial Age Transect' (PEAT), exploited the northward Pacific plate trajectory during the Cenozoic to recover a continuous sediment sequence from the equatorial Pacific. Cores from eight sites were obtained, from the sea floor to basaltic basement (that is, aged between 53 and 18 million years (Myr) before present), near the past position of the Equator at successive crustal ages on the Pacific plate[2]. Together with previous Deep Sea Drilling Project and Ocean Drilling Program drill cores, these sediments allow reconstruction of changes in the state, nature and variability of the global carbon cycle and climate system in unprecedented detail, from directly after the period of maximum Cenozoic warmth, through the onset of major glaciations, to the present.

Atmospheric CO_2 concentrations and climate are regulated on geological timescales by volcanic and metamorphic outgassing, weathering feedbacks involving the weathering of silicate and organic carbon (C_{org})-bearing rocks, and carbonate and C_{org} burial[3,4]. The integrated effect of these processes dictates the carbonate saturation state of the oceans that is reflected in the carbonate compensation depth (CCD), which has been highly influential in understanding past changes in the marine carbon cycle[5,6]. The CCD is a sediment property and occurs in the oceans where the downward flux of carbonate rain delivered from calcifying organisms is balanced by dissolution (Fig. 1), so that little or no carbonate is preserved in sediments below this depth. The CCD can be reconstructed using sediment cores[5–8].

Here we determine the evolution of the CCD by establishing the variation of net carbonate accumulation rates with respect to palaeodepth at multiple sites, using a common chronology and stratigraphic correlation. We then use carbon cycle models to explore viable mechanisms that may be responsible for the observed CCD variations; we highlight the importance of the supply of weathering-derived solutes to the deep ocean, and changes in the partitioning—into labile and refractory components—of organic matter delivered to deep-sea sediments.

A Cenozoic CCD record

Our new reconstruction of how the CCD in the equatorial Pacific region evolved through the Cenozoic is shown in Fig. 2a, and is compared with reconstructions of foraminiferal benthic $\delta^{18}O$ and $\delta^{13}C$ (Fig. 2b and c) and atmospheric CO_2 reconstructions (Fig. 2d) (Supplementary Fig. 1 shows this as a plot of mass accumulation rate against age and palaeo-latitude, Supplementary Fig. 2 shows an enlarged version for the Eocene). The evolving palaeo-position of

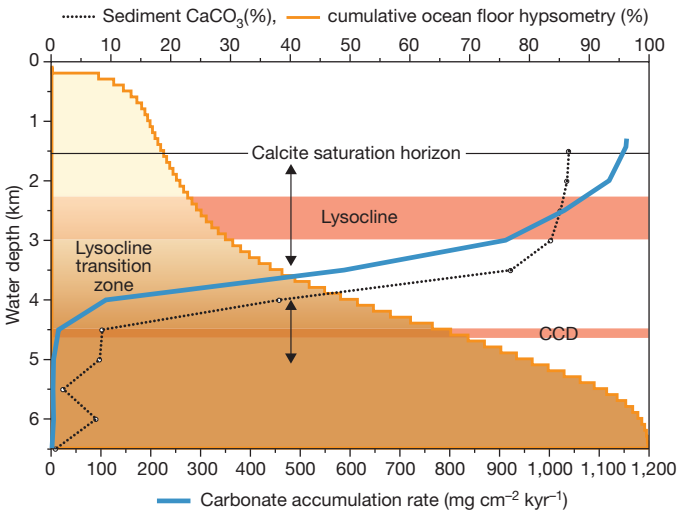

Figure 1 | Illustration of the position of the CCD and lysocline, and their relationship to ocean bathymetry, carbonate accumulation rate and $CaCO_3$ content. This figure shows the relationship between CCD, sediment $CaCO_3$ content (dotted black line), carbonate accumulation rate (blue line) and lysocline, in comparison with cumulative ocean floor hypsometry (orange line). The CCD, a sediment property, is defined as where carbonate rain is balanced by carbonate dissolution. Previously, it has been operationally defined to coincide with a fixed content of $CaCO_3$ (for example, 10%) in sediments[5], or where the carbonate accumulation rate interpolates to zero[6] (this second definition is advantageous as it is independent of non-carbonate supply or dilution effects). The lysocline is the horizon where dissolution becomes first noticeable (a sediment property), and is typically below the calcite saturation horizon.

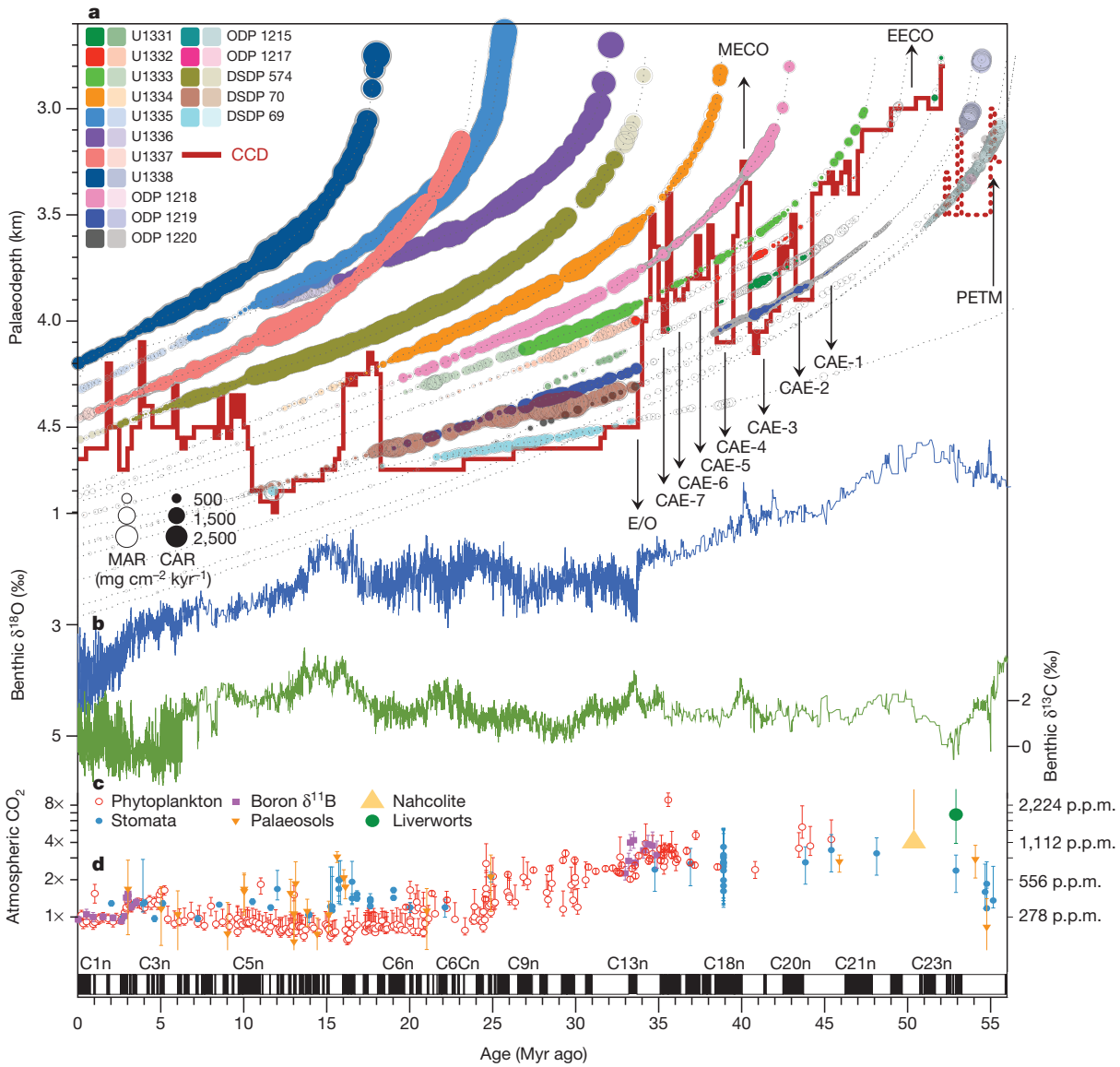

Figure 2 | CCD and carbonate accumulation rate reconstruction compared with published benthic foraminiferal $\delta^{18}O$ and $\delta^{13}C$ values and atmospheric CO_2. **a**, Equatorial Pacific accumulation rate history as a function of geological age at the backtracked and unloaded palaeo-water depth, and using a palaeomagnetic polarity age scheme[2] plotted as black and white bars below the figure. Circle area is scaled by accumulation rate: carbonate accumulation rate (CAR; filled circles), total mass accumulation rate (MAR; open circles). Data are plotted with a lighter colour outside a ±3.5° band around the palaeo-equator. The position of the equatorial Pacific CCD is indicated by a solid red line (dashed red line marks reconstruction from off-equatorial sites). See text for abbreviations. **b**, **c**, Benthic oxygen (**b**; blue curve, left-hand vertical axis) and carbon (**c**; green curve, right-hand vertical axis) isotope values from a global compilation[9], reported relative to the VPDB (Vienna Pee Dee Belemnite) standard. **d**, Atmospheric CO_2 compilation and error bars from refs 16, 40; left-hand vertical axis, log CO_2 scale relative to pre-industrial CO_2 (1× = 278 p.p.m.v.); right-hand vertical axis, log CO_2 scale in absolute values. Error bars are as in ref. 16; for example, for boron $\delta^{11}B$ error bars reflect long-term analytical reproducibility or internal precision, whichever is larger (at 95% confidence). PETM, Palaeocene-Eocene Thermal Maximum.

the CCD is determined as where the carbonate accumulation rates interpolated across the palaeo-depth transect reach zero as a function of depth. Overall, there is an intriguing correspondence of CCD deepening and deep ocean cooling[9], with a deepening from 3–3.5 km during the early Cenozoic to 4.6 km at present, consistent with findings of an overall Cenozoic increase in silicate weathering[10–13]. Superimposed on this overall deepening are repeated large CCD fluctuations during the middle and late Eocene.

We find that during the earliest Eocene (~56–53 Myr ago), the equatorial CCD generally occurred at a palaeo-depth of around 3.3–3.6 km, with superimposed 'hyperthermal'-related CCD shoaling events[9,14]. Between ~52 and 47 Myr ago, the CCD reached depths as shallow as 3 km, coincident with the Early Eocene Climatic Optimum (EECO)[15], when atmospheric CO_2 concentrations, including their uncertainty bounds, reached an estimated ~1,100–3,000 parts per million by volume (p.p.m.v.)[16], and the lowest benthic oxygen isotope values (indicating peak deep-ocean temperature) throughout the Cenozoic were attained[15].

From ~46 to 34 Myr ago, our record reveals a fluctuating and highly variable CCD[8], resolving 5–7 CCD deepenings and carbonate accumulation events (CAEs) with durations of several hundred thousand years to 1 Myr, interrupted by rapid CCD shoalings with an amplitude of ~0.5–1.0 km (CAE-1 to CAE-7; Fig. 2). The largest-magnitude fluctuation of the CCD during the middle and late Eocene coincided with carbonate accumulation event 3 (CAE-3)[8], followed by a near 1-km shoaling that is coeval with the Middle Eocene Climatic Optimum (MECO)[17,18]. A sustained large deepening (>1 km) then terminated a late Eocene interval of variability and

coincided with the Eocene/Oligocene (E/O) transition[19]. This terminal early Oligocene CCD deepening was contemporaneous with ice sheet growth, sea-level fall and a shift in carbonate deposition from shallow to deep waters[19,20]. The deeper (~4.6 km) and apparently more stable CCD of the Oligocene was interrupted again in the Miocene at ~18.5 Myr ago by a ~600-m shoaling, lasting for around 2.5 Myr, which was previously described as the "carbonate famine"[6]. The CCD deepened again to around 4.7 km at ~16 Myr ago as a consequence of increased carbonate productivity[6]. For this deepening event at ~16 Myr ago, the analysis of the PEAT data alone is complicated by the latitudinal movement of some sites (U1332–U1334) outside the Pacific equatorial zone (Supplementary Fig. 1). However, the interpretation is supported by previous work[6] and corroborated by large increases in carbonate mass accumulation rates at shallower depths of Sites U1335, U1337 and U1338 (Fig. 2). An interval with the deepest equatorial Pacific Cenozoic CCD of around 4.8 km was terminated by shoaling at ~10.5 Myr ago in a rapid "carbonate crash" event[21]. For the remainder of the Neogene, the equatorial Pacific CCD resided around 4.5 km depth with superimposed fluctuations in carbonate accumulation related to shorter-term climatic oscillations on Milankovitch timescales (20–400 kyr), as well as to the periodic deposition of diatom mats[2].

Eocene CCD fluctuations

Two features of the equatorial Pacific CCD behaviour during the Cenozoic stand out and demand further investigation. First, the Eocene CCD resided at an average depth of around 3.5 km, or ~1 km shallower than during post-Eocene time, with a geologically rapid and permanent deepening at the E/O transition. The E/O CCD deepening has previously been ascribed to ice expansion on Antarctica and sea-level fall, driving a shelf-to-basin shift in carbonate partitioning[19,20]. In contrast, for Eocene CAEs we lack evidence[22] for large bi-polar fluctuations in ice volume, so that alternative mechanisms must be explored.

Second, the middle to late Eocene was characterized by five major CCD fluctuations that lasted between 250 kyr and 1 Myr and had amplitudes between 200 and 900 m. The ~900-m CCD shoaling at ~40.5 Myr ago, a globally recognized feature[17] associated with the transition from CAE-3 to MECO, approaches the amplitude of (but is opposite in sign to) the CCD shift during the E/O transition from greenhouse to icehouse. We currently lack a definite confirmation that other CAEs are represented in records outside the equatorial Pacific, primarily owing to the scarcity of continuous, well-dated pelagic sedimentary records at an array of palaeo-depth positions, but we note that data from ODP Site 929E in the equatorial Atlantic tentatively support our hypothesis of CAEs as global features (Supplementary Fig. 3). In the equatorial Pacific, CAEs coincided with increased biogenic silica accumulation rates and shifts between calcareous and siliceous microfossils[8,18]. CAEs also coincided with enhanced burial of C_{org} in an Eocene Pacific Ocean otherwise characterized by productivity similar to today but with much faster water-column recycling; these increases in C_{org} burial start from a much lower Eocene baseline of C_{org} preserved in sediments, averaging only one-tenth of the present day value[8,23–25].

Carbon system modelling

To quantitatively explore the potential of different processes to generate the CCD signal reconstructed for the middle to late Eocene, we made use of steady-state results from an Earth system model of intermediate complexity (GENIE)[26,27], and investigated non-steady-state behaviour of shorter-lived processes with the palaeo-configuration of the LOSCAR box model[28] (Supplementary Information). Overall, the results from both models significantly reduce the number of possible mechanisms that are consistent with the reconstructed CCD history, either by demonstrating that a number of possible processes are not able to sustain large CCD changes over long enough time periods (>250 kyr), or by inconsistency with other proxy observations.

We start by assuming that middle–late Eocene CCD fluctuations represent alternating steady states of marine carbon cycling and that all carbonate weathering and climate feedbacks had time to operate and equilibrate. The justification for this is that the typical silicate weathering compensation time is of the order of ~0.1 Myr (refs 4, 29), much shorter than the duration of the reconstructed CCD fluctuations (0.25–1 Myr; Fig. 2). We then test the sensitivity of a range of established hypotheses for changing the CCD.

Processes we have investigated that either do not appear to be consistent with reconstructed amplitudes and durations of CCD shifts or are inconsistent with other proxy evidence (Supplementary Information) include: (1) C_{org} surface export rain ratio changes, which we exclude because the resultant CCD variations are too small in comparison to what we observe; (2) a shift in carbonate deposition between the shelf and deep ocean, for which a repeated large-scale oscillation in ice mass would be required that has so far not been observed; (3) a shift of deep ocean ventilation between a dominant Southern Ocean and dominant North Pacific source, which would lead to opposite CCD behaviour in different ocean basins; and (4) changes in deep-sea temperatures and the Mg and Ca concentration of sea water[4,9,30–32], which both modify the stability of calcium carbonate. For these, the CCD can be affected only by relatively subtle changes in the offset between CCD and lysocline because of the need to ultimately re-balance sources and sinks. We note that we cannot completely rule out the potential for ventilation changes to be compatible with our CCD data, and this will need to be resolved by future drilling in the North Atlantic.

Next, we focus on two model scenarios that do have the potential to sustain CCD changes of the required duration and amplitude: (1) perturbations to continental weathering and variations in solute input to the deep ocean, driving synchronous changes in CCD and lysocline depth globally, and/or (2) changes in the partitioning of C_{org} flux between labile and refractory components, affecting both deep-sea carbonate dissolution and the thickness of the lysocline transition zone (and hence partially decoupling the CCD from the lysocline).

To explore the first mechanism, we computed the steady-state CCD position in the equatorial Pacific through a range of atmospheric CO_2 values relative to pre-industrial modern ($1 \times CO_2 = 278$ p.p.m.v.) and against a range of solute weathering fluxes of Ca and HCO_3^- to the deep ocean in GENIE. Because in GENIE the solute flux to the deep ocean is the total weathering flux minus what is deposited on the shelves, changes in solute flux implicitly model either a change of the total flux, or shelf–basin partitioning. Our results (Fig. 3a) indicate that, for a given value of atmospheric CO_2, changes in solute flux to the deep ocean are in principle able to achieve changes in the equatorial Pacific CCD of the amplitude suggested by observations (several hundred metres to >1 km). For the Cenozoic, this supports the initial correlation between increased silicate weathering rates and CCD deepening.

However, other carbon cycle impacts resulting from the assumed driver of changes in solute supply must also be considered. On <1-Myr timescales, tectonic uplift is too slow, and there is no convincing evidence for repeated large-scale sea level fluctuations during the middle-to-late Eocene that could alternately shift the locus of carbonate deposition between shelf and deep ocean. Therefore, increasing solute supply should be coupled to increased weathering, a warmer climate and higher CO_2, unless changes in orbital configuration significantly enhance or reduce monsoon circulation (at constant CO_2), which could affect weathering fluxes via effects on precipitation intensity and distribution (which is not tested here). Our modelling reveals that increasing atmospheric CO_2 with fixed weathering (that is, with no weathering–temperature feedback enabled), results in a shallower CCD. This is a consequence of non-linearities in the carbonate system and reflects a deepening of the lysocline at the expense of the CCD and contraction of the lysocline

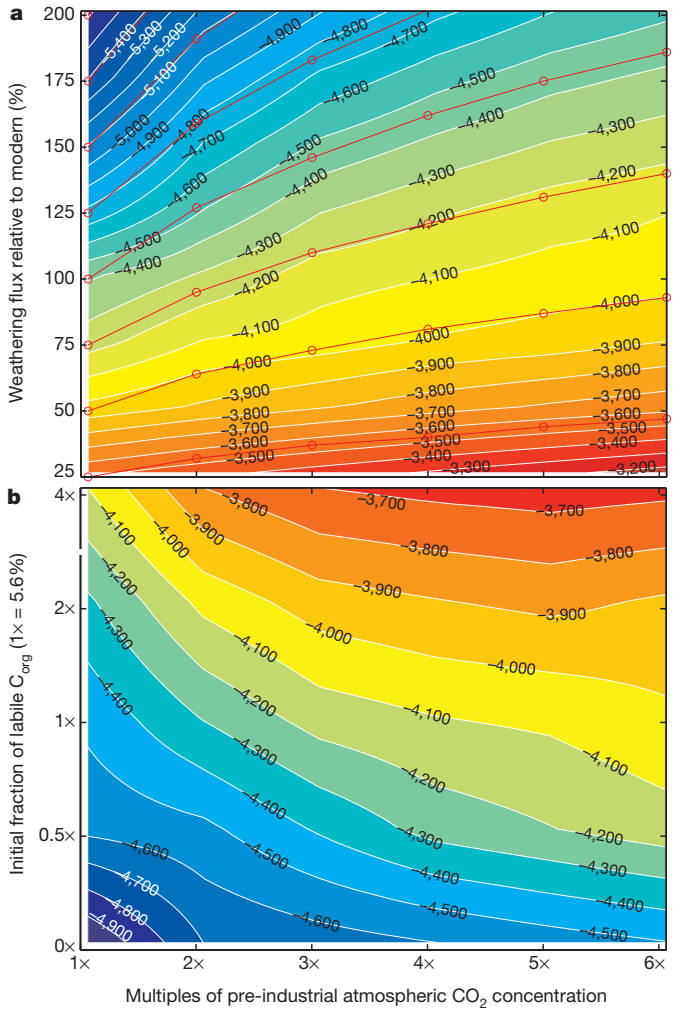

Figure 3 | CCD predicted by the GENIE steady state model. a, Eocene CCD plotted as contours (numbers show depth in m) as a function of atmospheric CO_2 concentrations (horizontal axis) and total net deep-sea weathering flux (compared to modern value of 10 Tmol yr^{-1}; vertical axis). All models were run without direct feedback on silicate weathering. The red lines indicate the increase in weathering flux when moving from 1× to 6× CO_2 silicate weathering feedback (using a partitioning of total initial weathering into silicate and carbonate weathering in a 1:1 ratio). **b**, As **a**, but plotting CCD as function of CO_2 (horizontal axis) and initial fraction of sediment labile C_{org} (vertical axis). This model ensemble was run with 100% net weathering compared to modern, and a surface $CaCO_3$:C_{org} rain ratio of 0.2.

transition zone. When this is combined with the response of increased weathering by activating the full silicate weathering feedback, we find an unexpected result: when progressively increasing the rate of prescribed CO_2 outgassing in a series of GENIE experiments, atmospheric CO_2 and weathering flux happen to co-vary in such a way that they result in a largely invariant CCD depth (Fig. 3a).

This result is subject to a number of model uncertainties and assumptions, including the degree of nonlinearity of weathering with climate, for which we have assumed a simple global-average response[29], and a 1:1 partitioning between carbonate and silicate weathering. The negative feedback in regulating atmospheric CO_2 on geological timescales due to weathering of continental materials had been included in the original BLAG[33] modelling study and is also used in GENIE and LOSCAR, but there are significant uncertainties attached to this parameterization. For example, the strength of this feedback has been shown to lead to significant variations in the carbon cycle response to weathering, but remains poorly constrained[29]. Although different weathering formulations were not tested with GENIE, we predict that the weak relationship between CCD and atmospheric CO_2 (Fig. 3a) probably indicates that additional silicate weathering changes in response to temperature will result in only small deviations from an invariant CCD after reaching steady state. Our results illustrate the non-intuitive nature of CCD behaviour and that higher marine carbonate deposition under a warmer, higher-CO_2 climate need not require a deeper observed CCD.

Independent observations of sediment composition and changes of dominant microfossil groups lead us to also assess whether changes in the behaviour of organic matter driving dissolution during the middle–late Eocene played a role. The pertinent observations are shifts between siliceous and calcareous microfossils and an increase of C_{org} burial flux during CAE-3, with simultaneous increased burial fluxes of calcareous and biosiliceous sediment[1,2,23–25]. For example, sediment smear slides from the equatorial Pacific reveal a major increase in diatom content from 0% to near 50% near the end of this event[24]. The relative changes in biogenic silica are much larger than those in calcareous plankton, and indicate major temporal reorganization of biotic composition rather than simple changes in productivity levels. In addition, the amount of C_{org} preserved in Eocene equatorial Pacific sediments is an order of magnitude smaller than today, despite a productivity that was not very different to the present[8,24], suggesting a more nutrient enriched deep ocean.

We investigate the viability of a 'sediment labile organic matter' hypothesis to help explain the CCD fluctuations. We repeat the GENIE net-weathering supply analysis but now change the partitioning between C_{org} that is redissolved in the upper water column and C_{org} that reaches the sea floor but is available to microbes to drive carbonate dissolution. This modifies the ocean's dissolved inorganic carbon as well as the net carbonate preservation flux[34]. This hypothesis builds on, but differs from, the classic glacial CO_2 rain ratio hypothesis[35], which postulated that changes in the $CaCO_3$ flux to ocean sediments, at a fixed particulate organic carbon (POC) supply, could be an effective way of changing atmospheric CO_2. However, the rebalancing of sedimentation versus weathering—carbonate compensation—while helping to drive a potential 60 p.p.m. fall in atmospheric CO_2 for a 40% decrease in $CaCO_3$:POC export ratio, also leads to a CCD that changed relatively little (Supplementary Fig. 5). This mechanism may also not be compatible with the consequence of any POC 'ballasting' by $CaCO_3$ (refs 36, 37).

Results for modelling the sediment labile organic matter hypothesis (Fig. 3b) indicate that a smaller initial fraction of labile organic matter results in a net increase in carbonate accumulation in regions of high productivity such as the eastern equatorial Pacific, Southern Ocean and equatorial Atlantic, owing to reduced water column dissolution. Carbonate compensation acts to mitigate the CCD changes but with a spatially heterogeneous pattern, leaving a deeper CCD in the eastern equatorial Pacific (Supplementary Fig. 9) and Atlantic, but resulting in smaller changes in the western Pacific. The modelled changes in carbonate accumulation in the eastern equatorial Pacific in this scenario indicate that CCD changes of ~300–600 m are possible for a 2–4-fold change in the initial fraction of sediment labile organic matter (Fig. 3b), roughly equivalent to the amplitude of all but the largest MECO-associated fluctuations in the record[17]. Although GENIE does not explicitly distinguish labile from refractory carbon delivered to the sediments, we are effectively assuming that surface biological productivity and the total flux of POC to deep-sea sediments need not change, but that it is either predominantly available for oxidation and driving carbonate dissolution (labile), or it is largely preserved and buried (refractory) and does not drive substantial additional carbonate dissolution.

CCD buffering

Overall, our modelling also reveals that the CCD is remarkably well buffered against short- and long-term perturbations of the global carbon cycle. Only a few of the mechanisms commonly envisaged

as important in controlling the CCD in practice have the capacity to change the amplitude of the steady-state CCD sufficiently and for long enough to be compatible with our reconstruction. In contrast, our labile organic matter hypothesis is consistent with shifts between siliceous and calcareous microfossil groups, and changes in C_{org} preservation and burial[24], and results in a large enough CCD shift to explain variability during the middle–late Eocene, perhaps in concert with simultaneous weathering flux changes. We note that the initial depth of the CCD may amplify these changes as its response to forcing is a function of the total amount of calcite available to be dissolved over a given depth range of sea floor (Supplementary Information and Supplementary Fig. 4). This suggests a smaller compensation capacity during Eocene time (due to a shallower CCD), which results in a higher sensitivity of carbonate preservation for a given carbon perturbation.

The Pacific CCD record presented here offers a new view of the evolution of Cenozoic ocean carbonate chemistry and provides the basis for future quantitative tests of multiple possible controlling mechanisms. The close correspondence of deep-ocean temperatures derived from benthic foraminiferal $\delta^{18}O$ records and the equatorial Pacific CCD is intriguing and suggests a close coupling of climate and carbon cycle feedbacks during the Cenozoic, tied to an overall increase in weathering during that time.

METHODS SUMMARY

Carbonate measurements were performed by coulometry[2], and supplemented with data from ODP and DSDP Legs (Supplementary Table 1). Accumulation rates were determined by using high-resolution age models and bulk dry density measurements. Stratigraphic correlation of sites was achieved through bio- and magnetostratigraphy, X-ray fluorescence data and physical property measurements[38], adjusted to the age model of the PEAT expeditions[2] revised to new site correlations[38]. Present-day site positions were backtracked using published stage poles[2]. Palaeo-depths were computed including backstripping and using standard methodology[6]. The CCD was semiquantitatively determined by plotting available carbonate accumulation rate data in 250-kyr windows, and fitting a regression line through carbonate accumulation rates decreasing with depth. GENIE Earth system modelling was based on Eocene boundary conditions from previous studies[26,27] using a Palaeocene palaeobathymetry (model SVN revision 7491). Scenarios were investigated as open system runs and with enabled climate feedback (temperature responsive to greenhouse gas forcing) until steady state conditions were achieved (~150 kyr). Ensembles were run on the University of Southampton high-performance computing system IRIDIS3. All scenarios were run for atmospheric CO_2 ranging from 1× to 6× pre-anthropogenic (1× = 278 p.p.m.v.). The scenario in Fig. 3a ('weathering') varied total weathering fluxes from 25% to 200% of modern DIC values in 25% steps (100% = 10 Tmol yr^{-1})[39]. For all runs bioturbation was switched off to speed up the achievement of steady state. All models were run adding a background wetland CH_4 flux at 5× pre-industrial levels, and with a constant detrital flux of 0.18 g cm^{-2} kyr^{-1}. The net-weathering scenario in Fig. 3a was then re-run with varying values for the initial fraction of labile organic carbon 'POM2' (standard GENIE value ~5.6%, additional runs with zero, half, double and quadruple standard value), detailed in a previous publication[34]. Additional GENIE scenarios are described in Supplementary Information.

Full Methods and any associated references are available in the online version of the paper.

Received 22 February; accepted 26 June 2012.

1. Lyle, M. *et al.* Pacific Ocean and Cenozoic evolution of climate. *Rev. Geophys.* **46,** RG2002, http://dx.doi.org/10.1029/2005RG000190 (2008).
2. Pälike, H. *et al.* Expedition 320/321 summary. *Proc. IODP* **320/321**, doi:10.2204/iodp.proc.320321.2010 (2010).
3. Broecker, W. S. & Peng, T.-H. The role of $CaCO_3$ compensation in the glacial to interglacial atmospheric CO_2 change. *Glob. Biogeochem. Cycles* **1,** 15–29 (1987).
4. Ridgwell, A. & Zeebe, R. The role of the global carbonate cycle in the regulation and evolution of the Earth system. *Earth Planet. Sci. Lett.* **234,** 299–315 (2005).
5. Van Andel, T. H., Heath, G. R. & Moore, T. C. Jr. Cenozoic history and paleoceanography of the central equatorial Pacific Ocean: a regional synthesis of Deep Sea Drilling Project data. *Geol. Soc. Am.* **143,** 1–134 (1975).
6. Lyle, M. Neogene carbonate burial in the Pacific Ocean. *Paleoceanography* **18,** 1059, http://dx.doi.org/10.1029/2002PA000777 (2003).
7. Peterson, L. C. & Backman, J. Late Cenozoic carbonate accumulation and the history of the carbonate compensation depth in the western equatorial Indian ocean. *Proc. ODP Sci. Res.* **115,** 467–508 (1990).
8. Lyle, M. W., Olivarez Lyle, A., Backman, J. & Tripati, A. Biogenic sedimentation in the Eocene equatorial Pacific—the stuttering greenhouse and Eocene carbonate compensation depth. *Proc. ODP Sci. Res.* **199,** 1–35 (2005).
9. Zachos, J. C., Dickens, G. R. & Zeebe, R. E. An early Cenozoic perspective on greenhouse warming and carbon-cycle dynamics. *Nature* **451,** 279–283 (2008).
10. Edmond, J. M. Himalayan tectonics, weathering processes, and the strontium isotope record in marine limestones. *Science* **258,** 1594–1597 (1992).
11. Lear, C. H., Elderfield, H. & Wilson, P. A. A Cenozoic seawater Sr/Ca record from benthic foraminiferal calcite and its application in determining global weathering fluxes. *Earth Planet. Sci. Lett.* **208,** 69–84 (2003).
12. Misra, S. & Froelich, P. N. Lithium isotope history of Cenozoic seawater: changes in silicate weathering and reverse weathering. *Science* **335,** 818–823 (2012).
13. Peucker-Ehrenbrink, B. & Ravizza, G. The marine osmium isotope record. *Terra Nova* **12,** 205–219 (2000).
14. Leon-Rodriguez, L. & Dickens, G. R. Constraints on ocean acidification associated with rapid and massive carbon injections: the early Paleogene record at Ocean Drilling Program Site 1215, equatorial Pacific Ocean. *Palaeogeogr. Palaeoclimatol. Palaeoecol.* **298,** 409–420 (2010).
15. Zachos, J. C., Pagani, M., Sloan, L., Thomas, E. & Billups, K. Trends, rhythms, and aberrations in global climate 65 Ma to present. *Science* **292,** 686–693 (2001).
16. Beerling, D. J. & Royer, D. L. Convergent Cenozoic CO_2 history. *Nature Geosci.* **4,** 418–420 (2011).
17. Bohaty, S. M., Zachos, J. C., Florindo, F. & Delaney, M. L. Coupled greenhouse warming and deep-sea acidification in the middle Eocene. *Paleoceanography* **24,** PA2207, http://dx.doi.org/10.1029/2008PA001676 (2009).
18. Spofforth, D. J. A. *et al.* Organic carbon burial following the middle Eocene climatic optimum in the central western Tethys. *Paleoceanography* **25,** PA3210, http://dx.doi.org/10.1029/2009PA001738 (2010).
19. Coxall, H. K., Wilson, P. A., Pälike, H., Lear, C. H. & Backman, J. Rapid stepwise onset of Antarctic glaciation and deeper calcite compensation in the Pacific Ocean. *Nature* **433,** 53–57 (2005).
20. Merico, A., Tyrrell, T. & Wilson, P. A. Eocene/Oligocene ocean de-acidification linked to Antarctic glaciation by sea-level fall. *Nature* **452,** 979–982 (2008).
21. Lyle, M. W., Dadey, K. & Farrell, J. The late Miocene (11–8 Ma) eastern Pacific carbonate crash: evidence for reorganization of deep-water circulation by the closure of the Panama Gateway *Proc. ODP Sci. Res.* **138,** 821–837 (1995).
22. Edgar, K. M., Wilson, P. A., Sexton, P. F. & Suganuma, Y. No extreme bipolar glaciation during the main Eocene calcite compensation shift. *Nature* **448,** 908–911 (2007).
23. Moore, T. C. Jr & Jarrard, R. D. Olivarez Lyle, A. & Lyle, M. W. Eocene biogenic silica accumulation rates at the Pacific equatorial divergence zone. *Paleoceanography* **23,** PA2202, http://dx.doi.org/10.1029/2007PA001514 (2008).
24. Olivarez Lyle, A. & Lyle, M. W. carbon and barium in Eocene sediments: possible controls on nutrient recycling in the Eocene equatorial Pacific Ocean *Proc. ODP Sci. Res.* **199,** 1–33 (2005).
25. Olivarez Lyle, A. & Lyle, M. W. Missing organic carbon in Eocene marine sediments: is metabolism the biological feedback that maintains end-member climates? *Paleoceanography* **21,** PA2007, http://dx.doi.org/10.1029/2005PA001230 (2006).
26. Panchuk, K., Ridgwell, A. & Kump, L. R. Sedimentary response to Paleocene-Eocene Thermal Maximum carbon release: a model-data comparison. *Geology* **36,** 315–318 (2008).
27. Ridgwell, A. & Schmidt, D. N. Past constraints on the vulnerability of marine calcifiers to massive carbon dioxide release. *Nature Geosci.* **3,** 196–200 (2010).
28. Zeebe, R. E. LOSCAR: Long-term Ocean-atmosphere-Sediment CArbon cycle Reservoir Model v2.0.4. *Geoscientific Model Dev.* **5,** 149–166 (2012).
29. Uchikawa, J. & Zeebe, R. E. Influence of terrestrial weathering on ocean acidification and the next glacial inception. *Geophys. Res. Lett.* **35,** L23608, http://dx.doi.org/10.1029/2008GL035963 (2008).
30. Coggon, R. M., Teagle, D. A. H., Smith-Duque, C. E., Alt, J. C. & Cooper, M. J. Reconstructing past seawater Mg/Ca and Sr/Ca from mid-ocean ridge flank calcium carbonate veins. *Science* **327,** 1114–1117 (2010).
31. Stuecker, M. F. & Zeebe, R. E. Ocean chemistry and atmospheric CO_2 sensitivity to carbon perturbations throughout the Cenozoic. *Geophys. Res. Lett.* **37,** L03609, http://dx.doi.org/10.1029/2009GL041436 (2010).
32. Tyrrell, T. & Zeebe, R. History of carbonate ion concentration over the last 100 million years. *Geochim. Cosmochim. Acta* **68,** 3521–3530 (2004).
33. Berner, R. A., Lasaga, A. C. & Garrels, R. M. The carbonate-silicate geochemical cycle and its effect on atmospheric carbon dioxide over the past 100 million years. *Am. J. Sci.* **283,** 641–683 (1983).
34. Ridgwell, A. *et al.* Marine geochemical data assimilation in an efficient Earth System Model of global biogeochemical cycling. *Biogeosciences* **4,** 87–104 (2007).
35. Archer, D. & Maier-Reimer, E. Effect of deep-sea sedimentary calcite preservation on atmospheric CO_2 concentration. *Nature* **367,** 260–263 (1994).
36. Armstrong, R. A., Lee, C., Hedges, J. I., Honjo, S. & Wakeham, S. G. A new, mechanistic model for organic carbon fluxes in the ocean: based on the quantitative association of POC with ballast minerals. *Deep Sea Res. II* **49,** 219–236 (2001).
37. Ridgwell, A. An end to the "rain ratio" reign? *Geochem. Geophys. Geosyst.* **4,** 1051, http://dx.doi.org/10.1029/2003GC000512 (2003).
38. Westerhold, T. *et al.* Revised composite depth scales and integration of IODP Sites U1331–U1334 and ODP Sites 1218–1220. *Proc. IODP* **320/ 321,** 1–137 (2012).

39. Archer, D. Modeling the calcite lysocline. *J. Geophys. Res. C* **96,** 17037–17050 (1991).
40. Pagani, M. *et al.* The role of carbon dioxide during the onset of Antarctic glaciation. *Science* **334,** 1261–1264 (2011).

Supplementary Information is available in the online version of the paper.

Acknowledgements This research used samples and data provided by IODP. We thank the masters and crew of IODP Expeditions 320 and 321. H.P. acknowledges support from the Philip Leverhulme Prize, the BIK-F, and NERC grants NE/H000089/1, NE/H020136/1, NE/G003270/1, NE/F003641/1, NE/H022554/1 and NE/I006168/1. We acknowledge the use of the IRIDIS High Performance Computing Facility, and associated support services at the University of Southampton, in the completion of this work. We thank M. Palmer and D. Teagle for discussions. E.J.R. is a Visiting Fellow at the Research School of Earth Sciences, The Australian National University.

Author Contributions H.P. and A.R. wrote the manuscript. H.P., A.R., C.O.J.C. and R.E.Z. contributed to the modelling work. All authors contributed to data analysis, interpretation, manuscript editing or discussions.

Author Information Reprints and permissions information is available at www.nature.com/reprints. The authors declare no competing financial interests. Readers are welcome to comment on the online version of the paper. Correspondence and requests for materials should be addressed to H.P. (hpaelike@marum.de).

Heiko Pälike[1], Mitchell W. Lyle[2], Hiroshi Nishi[3], Isabella Raffi[4], Andy Ridgwell[5], Kusali Gamage[6], Adam Klaus[6], Gary Acton[7], Louise Anderson[8], Jan Backman[9], Jack Baldauf[2], Catherine Beltran[10], Steven M. Bohaty[1], Paul Bown[11], William Busch[12], Jim E. T. Channell[13], Cecily O. J. Chun[1,14,15], Margaret Delaney[16], Pawan Dewangan[17], Tom Dunkley Jones[18,19], Kirsty M. Edgar[1,20], Helen Evans[21], Peter Fitch[18], Gavin L. Foster[1], Nikolaus Gussone[22], Hitoshi Hasegawa[23], Ed C. Hathorne[24], Hiroki Hayashi[25], Jens O. Herrle[14,15], Ann Holbourn[26], Steve Hovan[27], Kiseong Hyeong[28], Koichi Iijima[29], Takashi Ito[30], Shin-ichi Kamikuri[31,32], Katsunori Kimoto[33], Junichiro Kuroda[34], Lizette Leon-Rodriguez[35], Alberto Malinverno[21], Ted C. Moore Jr[36], Brandon H. Murphy[37], Daniel P. Murphy[1,2], Hideto Nakamura[31], Kaoru Ogane[38], Christian Ohneiser[39], Carl Richter[40], Rebecca Robinson[41], Eelco J. Rohling[1], Oscar Romero[42], Ken Sawada[31], Howie Scher[43], Leah Schneider[44], Appy Sluijs[45], Hiroyuki Takata[46], Jun Tian[47], Akira Tsujimoto[48], Bridget S. Wade[49,50], Thomas Westerhold[51], Roy Wilkens[52], Trevor Williams[21], Paul A. Wilson[1], Yuhji Yamamoto[32], Shinya Yamamoto[53], Toshitsugu Yamazaki[54] & Richard E. Zeebe[55]

[1]Ocean and Earth Science, National Oceanography Centre Southampton, University of Southampton, Waterfront Campus, European Way, Southampton SO14 3ZH, UK. [2]Department of Oceanography, Texas A&M University, College Station, Texas 77840-3146, USA. [3]The Center for Academic Resources and Archives, Tohoku University Museum, Tohoku University, Aramaki Aza Aoba 6-3, Aoba-ku, Sendai 980-8578, Japan. [4]Dipartimento di Geotecnologie per l'Ambiente e il Territorio, DiGAT–CeRS Geo, Universitá ''G. DAnnunzio'', Campus Universitario, via dei Vestini 31, Chieti Scalo, Italy. [5]School of Geographical Sciences, University of Bristol, University Road, Bristol BS8 1SS, UK. [6]Integrated Ocean Drilling Program, Texas A&M University, 1000 Discovery Drive, College Station, Texas 77845-9547, USA. [7]Department of Geology, University of California, Davis, One Shields Avenue, Davis, California 95616, USA. [8]Department of Geology, University of Leicester, Leicester LE1 7RH, UK. [9]Department of Geological Sciences, Stockholm University, SE-10691 Stockholm, Sweden. [10]UPMC-Université Paris 06, ISTeP, UMR 7193-4 Place Jussieu, 75252 Paris Cedex 05, France. [11]Earth Sciences, University College London, Gower Street, London WC1E 6BT, UK. [12]Earth and Environmental Sciences, University of New Orleans, 2000 Lakeshore Drive, New Orleans, Louisiana 70148, USA. [13]Department of Geological Sciences, University of Florida, 241 Williamson Hall, Gainesville, Florida 32611-2120, USA. [14]Institute of Geosciences, Goethe University Frankfurt, Altenhöferallee 1, D-60438 Frankfurt, Germany. [15]Biodiversity and Climate Research Centre (BIK-F), and Senckenberg Gesellschaft für Naturforschung, D-60325 Frankfurt, Germany. [16]Ocean Sciences, University of California, Santa Cruz, 1156 High Street, Santa Cruz, California 95064, USA. [17]National Institute of Oceanography, Dona Paula, Goa 403 004, India. [18]Imperial College London, Department of Earth Science and Engineering, South Kensington Campus, London SW7 2AZ, UK. [19]School of Geography, Earth and Environmental Sciences, University of Birmingham, Edgbaston, Birmingham B15 2TT, UK. [20]School of Earth and Ocean Sciences, Cardiff University, Main Building, Park Place, Cardiff CF10 3AT, UK. [21]Lamont-Doherty Earth Observatory of Columbia University, PO Box 1000, 61 Route 9W, Palisades, New York 10964, USA. [22]Institut für Mineralogie, Westfälische Wilhelms-Universität Münster, Corrensstrasse 24, 48149 Münster, Germany. [23]Department of Natural History Science, Graduate School of Science, Hokkaido University, N10W8, Kita-ku, Sapporo 060-0810, Japan. [24]GEOMAR, Helmholtz Centre for Ocean Research Kiel, Wischhofstrasse 1-3, 24148 Kiel, Germany. [25]Interdisciplinary Faculty of Science and Engineering, Shimane University, 1060 Nishikawatsucho, Matsue City, Shimane 690-8504, Japan. [26]Institut für Geowissenschaften, Christian-Albrechts-Universität zu Kiel, Olshausenstrasse 40, 24098 Kiel, Germany. [27]Department of Geoscience, Indiana University of Pennsylvania, 114 Walsh Hall, Indiana, Pennsylvania 15705, USA. [28]Deep Sea Resources Research Center, Korea Ocean Research and Development Institute, ANSAN PO Box 29, Seoul 425-600, Korea. [29]Institute of Biogeosciences, Japan Agency for Marine-Earth Science and Technology, 2-15 Natsushima-cho, Yokosuka 237-0061, Japan. [30]Faculty of Education, Ibaraki University, 2-1-1 Bunkyo, Mito, Ibaraki 310-8512, Japan. [31]Faculty of Science, Division of Natural History Sciences, Hokkaido University, Kita-10, Nishi-8, Kita-ku, Sapporo 060-0810, Japan. [32]Center for Advanced Marine Core Research, Kochi University, Kochi 783-8502, Japan. [33]Research Institute for Global Change (RIGC), JAMSTEC, 2-15 Natsushima-Cho, Yokosuka 237-0061, Japan. [34]Institute for Frontier Research on Earth Evolution (IFREE), JAMSTEC, 2-15 Natsushima-cho, Yokosuka 237-0061, Japan. [35]Department of Earth Science, Rice University, 6100 Main Street, MS-126, Houston, Texas 77005, USA. [36]Department of Geological Sciences, University of Michigan, 1100 North University, Ann Arbor, Michigan 48109-1005, USA. [37]Earth and Planetary Sciences, University of California, Santa Cruz, 1156 High Street, Santa Cruz, California 95064, USA. [38]Institute of Geology and Paleontology, Tohoku University, Aoba 6-4, Aramaki, Aoba-ku, Sendai City 980-8578, Japan. [39]Department of Geology, University of Otago, PO Box 56, Dunedin, New Zealand. [40]School of Geosciences, University of Louisiana, PO Box 44530, Lafayette, Louisiana 70504-0002, USA. [41]Graduate School of Oceanography, University of Rhode Island, South Ferry Road, Narragansett, Rhode Island 02882, USA. [42]Instituto Andaluz de Ciencias de la Tierra, Universidad de Granada, Campus Fuentenueva, 18002 Granada, Spain. [43]Department of Earth and Ocean Sciences, 701 Sumter Street, EWS 617 University of South Carolina, Columbia, SC 29208, USA. [44]Department of Geosciences, Pennsylvania State University, 509 Deike Building, University Park, Pennsylvania 16802, USA. [45]Department of Earth Sciences, Faculty of Geosciences, Utrecht University, Laboratory of Palaeobotany and Palynology, Budapestlaan 4, 3584CD Utrecht, The Netherlands. [46]BK21 Coastal Environmental System School, Division of Earth Environmental System, Pusan National University, San 30 Jangjeon-dong, Geumjeong-gu, Busan 609-735, Korea. [47]State Key Laboratory of Marine Geology, Tongji University, Siping Road 1239, Shanghai 200092, China. [48]Faculty of Education, Shimane University, 1060 Nishikawatsucho, Matsue City, Shimane 690-8504, Japan. [49]Department of Geology and Geophysics, Texas A&M University, College Station, Texas 77843-3115, USA. [50]School of Earth and Environment, University of Leeds, Woodhouse Lane, Leeds LS2 9JT, UK. [51]Center for Marine Environmental Sciences (MARUM), University of Bremen, 28359, Bremen, Germany. [52]Hawaii Institute of Geophysics and Planetology, University of Hawaii at Manoa, 1680 East West Road, Honolulu, Hawaii 96822, USA. [53]Yamanashi Institute of Environmental Sciences, 5597-1 Kenmarubi, Kamiyoshida, Fujiyoshida, Yamanashi 403-0005, Japan. [54]Geological Survey of Japan, AIST, 1-1-1 Higashi, Tsukuba, Ibaraki 305-8567, Japan. [55]School of Ocean and Earth Science and Technology, Department of Oceanography, University of Hawaii at Manoa, 1000 Pope Road, MSB 504, Honolulu, Hawaii 96822, USA.

METHODS

Data generation. Carbonate measurements were performed by coulometry during IODP Expeditions 320/321[2], and supplemented with previously published data from ODP and DSDP Legs (Supplementary Table 1). Mass and carbonate accumulation rates were determined by using high-resolution age models and bulk dry density measurements. Stratigraphic correlation of sites was achieved through bio- and magnetostratigraphy, XRF data and physical property measurements[38], and all data are adjusted to the age model of the PEAT expeditions[2]. Present-day site positions were backtracked using published stage poles[2]. Palaeo-depths were computed assuming subsidence proportional to the square root of age, following previous approaches[6], starting from an assumed ridge crest depth of 2.75 km, and taking into account sediment loading. Uncertainties in the palaeo-depth history are a function of (1) age control, (2) knowledge of the palaeo-depth of the ridge crest, (3) the subsidence history of drill sites, and (4) the sediment loading history for each site. For this study, we assumed a palaeo-depth of the ridge of 2.75 km, fitted subsidence parameters according to the determined basement age and present-day depth and backstripped the sediment loading following previous work[6]. Age models for individual sites are based on an integrated palaeomagnetic and biostratigraphic framework largely following the Expedition dates[2], but revised to new site correlations[38]. Biostratigraphic ages from previous ODP and DSDP sites were updated to this age framework. The new carbonate compensation depths were semiquantitatively determined by plotting available carbonate accumulation rate data in 250-kyr windows, and fitting a regression line through the carbonate accumulation rates that are decreasing with depth.

Earth system modelling. GENIE Earth system modelling was based on previous studies[26,27] using a Palaeocene palaeobathymetry, using model SVN revision 7491 (contact authors for detailed access information). Scenarios were investigated as open system runs and with enabled climate feedback (temperature responsive to greenhouse gas forcing) until steady state conditions were achieved (~150 kyr), using the following Eocene boundary conditions[27]: a solar constant reduced by 0.46% for Palaeogene time (1,361.7 W m^{-2}); a reduced salinity of 33.9 p.s.u.; a constant $CaCO_3$:C_{org} ratio of 0.2, and with seawater concentrations of Mg ≈ 30 mmol kg^{-1} and Ca ≈ 15 mmol kg^{-1}. Ensembles were run on the Southampton high performance computing system IRIDIS3. All scenarios were run for atmospheric CO_2 concentrations ranging from 1× to 6× pre-anthropogenic (1 × = 278 p.p.m.v.). Bottom water temperatures in the model runs corresponding to increasing CO_2 levels are (in °C) 6.6, 9.4, 11.1, 12.3, 13.3 and 14.2, respectively. For all runs bioturbation was switched off to speed up the achievement of steady state. All models were run adding a background wetland CH_4 flux at 5× pre-industrial levels, and with a constant detrital flux of 0.18 g cm^{-2} kyr^{-1}. The scenario in Fig. 3a ('weathering') varied total weathering fluxes from 25% to 200% of modern DIC values in 25% steps (100% = 10 Tmol yr^{-1})[39]. The net-weathering scenario in Fig. 3a was then also re-run with varying values for the initial fraction of labile organic carbon parameter 'POM2' (detailed in ref. 34, standard GENIE value ~5.6%, additional runs with zero, half, double and quadruple standard value). Results from further GENIE scenario runs not resulting in large CCD changes (rain ratio and Mg/Ca changes) are detailed in Supplementary Information, and we also include a description of transient model runs using the LOSCAR box model[28]. For the supplementary 'rain ratio' scenario we varied $CaCO_3$:C_{org} ratios from 0.1 to 0.225 in 0.025 steps, using a fixed 50% modern weathering supply to the deep ocean. A supplementary 'Mg/Ca' scenario varied seawater Mg and Ca concentrations using previously published values[32] for a Mg/Ca range from 1.3 to 5.1, also using a 50% weathering flux compared to modern.

Palaeo-depth uncertainties. The vertical uncertainty of palaeo-depth trajectories is likely to be largest for the earliest part of our records, attributable to the initially more rapid thermal cooling and subsidence at the palaeo-ridge (basement age error ±0.5 Myr), and due to absolute uncertainties in the palaeo-depth of the ridge crest (depth error ±350 m)[41]. Reconstructions become more robust for each site moving forward in time, as the thermal subsidence rate attenuates. We therefore estimate the uncertainty of absolute site palaeo-depths to be of the order of several hundred metres in the early part of the reconstruction for each site, and ~250 m for the remaining record. The palaeo-depth-transect approach however, means that most of the included sites originate from the same Pacific plate ridge segment, thereby reducing the relative error of depth reconstructions.

41. Calcagno, P. & Cazenave, A. Subsidence of the sea-floor in the Atlantic and Pacific Oceans — regional and large-scale variations. *Earth Planet. Sci. Lett.* **126,** 473–492 (1994).